archives
of thermodynamics
Vol. **40**(2019), No. 3, 3–26
DOI: 10.24425/ather.2019.129547

Mathematical modeling of hydrogen production performance in thermocatalytic reactor based on the intermetallic phase of Ni_3Al

JANUSZ BADUR[a]
MICHAŁ STAJNKE[a]
PAWEŁ ZIÓŁKOWSKI[b*]
PAWEŁ JÓŹWIK[c]
ZBIGNIEW BOJAR[c]
PIOTR JÓZEF ZIÓŁKOWSKI[a,d]

[a] Institute of Fluid Flow Machinery Polish Academy of Sciences, Energy Conversion Department, Fiszera 14, 80-231 Gdańsk, Poland

[b] Gdańsk University of Technology, Faculty of Mechanical Engineering, Narutowicza 11/12, 80-233 Gdańsk, Poland

[c] Faculty of Advanced Technologies and Chemistry, Military University of Technology, Kaliskiego 2., 00-908 Warszawa, Poland

[d] Faculty of Civil and Environmental Engineering, Gdańsk University of Technology, Narutowicza 11/12, 80-233 Gdańsk, Poland

Abstract The main goal of the considered work is to adjust mathematical modeling for mass transfer, to specific conditions resulting from presence of chemical surface reactions in the flow of the mixture consisting of helium and methanol. The thermocatalytic devices used for decomposition of organic compounds incorporate microchannels coupled at the ends and heated to 500 °C at the walls regions. The experiment data were compared with computational fluid dynamics results to calibrate the constants of the model's user defined functions. These extensions allow to transform the calculations mechanisms and algorithms of commercial codes adapting

*Corresponding Author. Email: pawel.ziolkowski1@pg.edu.pl, pawel.ziolkowski@imp.gda.pl

them for the microflows cases and increased chemical reactions rate on the interphase between fluid and solid, specific for catalytic reactions. Results obtained on the way of numerical calculations have been calibrated and compared with the experimental data to receive satisfactory compliance. The model has been verified and the performance of the thermocatalytic reactor with microchannels under hydrogen production regime has been investigated.

Keywords: Thermal decomposition; Spiecies transport; Catalyst; CFD

Nomenclature

A	–	surface area, m^2
$D_{mm'}$	–	coefficient of multicomponents diffusion
D_m^T	–	coefficient of temperature diffusion
e	–	total specific energy, $\frac{\mathrm{J}}{\mathrm{kg}}$
$\mathbf{e}_i$	–	versor in $\boldsymbol{i}$-direction
H	–	distance from the centre of microchannel (point O), mm
$\mathbf{I}$	–	unit tensor ($=\delta_{ij}\mathbf{e}_i \otimes \mathbf{e}_j$)
$\mathbf{J}_m$	–	diffusive flux of mixture component, $\frac{\mathrm{kg}}{\mathrm{s\ m^2}}$
$\mathbf{J}_k$	–	diffusive flux of turbulent kinetic energy, $\frac{\mathrm{m^2}}{\mathrm{s^2}} \frac{1}{\mathrm{s\ m^2}}$
$\mathbf{J}_\varepsilon$	–	diffusive flux of dissipation of turbulent kinetic energy, $\frac{\mathrm{m^2}}{\mathrm{s^3}} \frac{1}{\mathrm{s\ m^2}}$
k	–	kinetic energy of turbulence, $\frac{\mathrm{m^2}}{\mathrm{s^2}}$
$k_{(\alpha)}$	–	forward rate constant for volumetric reaction, $\frac{1}{\mathrm{s}}$
k_{cat}	–	thermocatalytic decomposition rate constant, $\frac{\mathrm{m^3}}{\mathrm{m^2_{cat}\,s}}$
L	–	length along reactor, mm
m	–	components of mixture (m = He, CH_3OH, CO, H_2, CH_4, H_2O, CO_2)
|OL|	–	long straight in cross section, m
|OS|	–	short straight in cross section, m
p	–	thermodynamic pressure, Pa
$\mathbf{q}^t$	–	total diffusive heat flux, $\frac{\mathrm{W}}{\mathrm{m^2}}$
$q_{(\alpha)}$	–	the progression level of αth chemical reaction
S_e, S_k, S_ε, S_m	–	sources of energy; turbulent kinetic energy; dissipation of turbulent kinetic energy; mixture component, respectively, $\frac{\mathrm{W}}{\mathrm{kg}}$, $\frac{m^2}{\mathrm{s^3}}$, $\frac{m^2}{\mathrm{s^4}}$, $\frac{1}{\mathrm{s}}$
$\mathbf{S_v}$	–	momentum sources, $\frac{\mathrm{m}}{\mathrm{s^2}}$
t	–	time, s
$\mathbf{t}^t$	–	total diffusive momentum flux (laminar and turbulent) ($=\mathbf{t}^{lam}+\mathbf{t}^{tur}$)
u	–	specific internal energy, $\frac{\mathrm{J}}{\mathrm{kg}}$
$\mathbf{V}_m$	–	diffusion velocity, $\frac{\mathrm{m}}{\mathrm{s}}$
V	–	volume, m^3

$\mathbf{v}$	–	velocity vector ($=v_i\mathbf{e}_i$)
v_i	–	value of velocity vector component, $\frac{\mathrm{m}}{\mathrm{s}}$
X_m	–	mole fraction, $\frac{\mathrm{kmol}}{\mathrm{kmol}}$
T	–	temperature, K
$\mathbf{x}$	–	placement
$[X_m]$	–	molar concentration, $\frac{\mathrm{mol}}{\mathrm{m}^3}$
Y_m	–	mass fraction of gas component, $\frac{\mathrm{kg}}{\mathrm{kg}}$
$\overline{W}$	–	average molecular weight, $\frac{\mathrm{kg}}{\mathrm{kmol}}$
$W_{\mathrm{CH_3OH}}$	–	molecular mass of methanol, $\frac{\mathrm{kg}}{\mathrm{kmol}}$
W_m	–	molecular weight of gas component, $\frac{\mathrm{kg}}{\mathrm{kmol}}$
$W_{m'}$	–	molecular mass of component $m' \neq m$, $\frac{\mathrm{kg}}{\mathrm{kmol}}$
$\otimes$	–	symbol of dyadic multiplication

Greek symbols

α_{cat}	–	factor of influence of 'third body'
δ_{ij}	–	Kronecker's delta
ε	–	dissipation of kinetic energy of turbulence, $\frac{m^2}{\mathrm{s}^3}$
$\nu_{m(\alpha)}$	–	stoichiometric matrix coefficients
$\nu_{\mathrm{CH_3OH}\ (\alpha)}$	–	molar stoichiometric coefficient for CH_3OH and αth reaction
ρ	–	mixture density ($=\rho(\mathbf{x},t)$), $\frac{\mathrm{kg}}{\mathrm{m}^3}$

Subscripts and superscripts

α	–	number of chemical reaction, $(\alpha)=1,2,3$
cat	–	catalytic
$cell$	–	computational cell
ε	–	dissipation of kinetic energy of turbulence
$i,\ j$	–	$i,\ j=1,2,3$ or $i,\ j=x,y,z$ (Cartesian coordinates)
k	–	turbulent kinetic energy
m,m'	–	components of mixture
mm'	–	interaction of components of mixture $m \neq m$'
lam	–	laminar
T	–	temperature
t	–	total
tur	–	turbulent

Abbreviation

CFD	–	computational fluid dynamics
CFM	–	computational flow mechanics
UDFs	–	user defined functions

1 Introduction

Current issues of the environmentally friendly, sustainable energy sources become increasingly important, and hydrogen is one of the most promising solutions [1–3]. Hydrogen can be employed in many devices for energy conversion and produced in many different ways which enables its wide

application, for example in hybrid cycle solid oxide fuel cell/gas turbine [4–5]. Furthermore, hydrogen can be considered as an accessible and natural renewable energy source [6]. Hydrogen can be produced by chemical reaction at elevated temperature and in the presence of catalysts. Such applications for thermocatalytic reactors in which the role performed by the active nickel-based materials have recently been explored by Jóźwik *et al.* [7–8].

Among others, Ni-based catalysts exhibit extremely high catalytical activity in methanol decomposition and other gasses synthesis and promote the production of carbon nanostructures (mainly carbon nanotubes) [7,9]. One of the Ni-based, solid-state catalysts is the Ni_3Al intermetallic phase and its alloys [8], which belongs to a sort of multifunctional materials, combining properties of both the structural and functional materials. They are resistant to oxidation and corrosion at normal condition, have a relatively low density and a relatively high melting point. Additionally, these materials retain sufficient strength at elevated temperatures and are relatively easy to be formed [10]. According to literature, Ni_3Al intermetallic thin foils exhibit extremely high catalytic properties in hydrocarbon decomposition reactions [11]. One example of an alloy foil package based on the intermetallic phase Ni_3Al, constructed as a rolled up honeycomb structure, is shown in Fig. 1, where the foil thickness is compared to the thickness of a human hair.

The appropriate selection of the dimensions of the device, in such way that the contact time of the flow across the catalytically active surface of the substrate providing the reaction of the target product, is very important. In addition to experimental studies, some work focused on the modeling of thermocatalytic processes is becoming increasingly interesting. Besides these works, that describe in general the processes of chemical reactions [12] there are articles concerning models of reactors and catalytic microreactors [13]. As has been demonstrated in recent works [13,14] in modeling flows with a strong interaction of surface and liquid material, boundary conditions and appropriate closure in mathematical models are essential. It should be mentioned that the huge surface-to-volume ratio has turned researchers attention to the fundamental understanding of the nature of 'surface-type driving forces' and the variety of different 'jump' phenomena like slipping, rolling, spin-slipping, surface mobility, surface friction, thermo-porosis, etc. Nonetheless, in the paper by Jóźwik *et al.* [13] the concept had emerged that within given operating conditions and the given

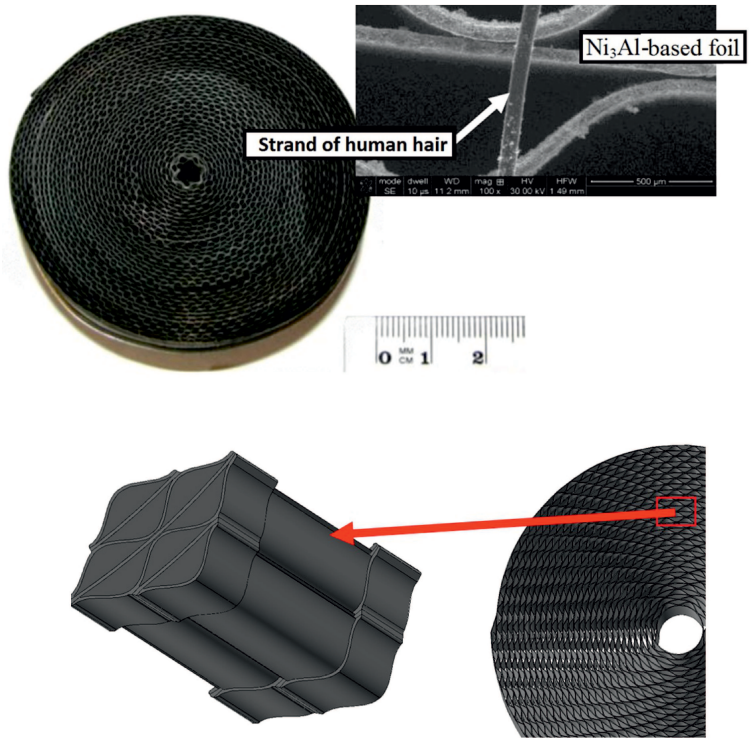

Figure 1: The alloy foil package based on the Ni_3Al intermetallic phase rolled into a honeycomb with zoomed foil and geometry of the eight single microchannels beginning at inlet into the package and terminating at the outlet from the package.

geometry of the microreactor, there is no need for the application of slip boundary conditions. Moreover Knudsen diffusion is not considered in this paper with respect to the modeling of this thermocatalytic microreactor. Hence, within the mentioned work [13] it has also been shown that the microreactor's length could be practically estimated using standard models.

This paper is a continuation of the analysis within the geometry of a single package of microchannels (Figs. 1 and 2) [13]. The alloy foil package based on the Ni_3Al intermetallic phase rolled into a honeycomb with zoomed foil and geometry of the eight single microchannels beginning at inlet into the package and terminating at the outlet from the package is presented in Fig. 1. However, different issues have been considered, namely the catalytic surface reactions of the decomposition of methanol and the

volume reaction of shifting or methanation inside the microchannel.

The main focus of this paper is to describe the mathematical modeling of momentum, heat and mass transfer, which is accompanied by the chemical surface reactions of the flow of helium and methanol mixtures. The thermocatalytic devices used for the decomposition of hydrocarbons incorporates vertical microchannel coupled at the ends which are heated to 500 °C at the walls. The results of this experiment were compared with computational fluid dynamics (CFD) simulations to calibrate the constants of the model user defined functions (UDFs). These extensions transformed the calculations, mechanisms and algorithms of the commercial codes, adapting them for the microflow cases and increased chemical reaction rates on the interphase between fluid and solid. Results obtained on the way of numerical calculations have been calibrated and compared with the experimental data to receive satisfactory accordance. The model has been verified and the performance of the thermocatalytic reactor with microchannels within the hydrogen production regime has been investigated.

2 Computational fluid dynamics governing equations

Classical CFD allows for the modeling of heat transfer, chemical and electrochemical reactions as fluid flow processes in devices of different types. Looking at the applications, which evolve more complex volumetric and surface phenomena such as advanced heat transfer [15,16], phase transition [17,18], nanoflows [19,20], complex chemical reaction [21,22] and the degradation of elements of power plants [23], many different papers have, in recent years, been prepared by numerous researchers. However, particular emphasis should be placed on the generating the additional terms necessary for the modeling of surface catalytic reactions [24,25]. The model of the catalytic reaction of methanol decomposition on the surface of alloys based on the intermetallic phase of Ni_3Al has been described in the previous studies by Moussa and El-Shall [11] and Xu *et al.* [25]. The best example of catalytic reaction is combustion in a honeycombed set of microchannels, which has been described in a previous study by Jóźwik *et al.* [13]. A similar geometrical set, namely the microchannels, has also been employed in the present consideration. The microreactor generally consists of minichannels (microchannels) which are separated by a thin solid wall, as is presented schematically in Fig. 2.

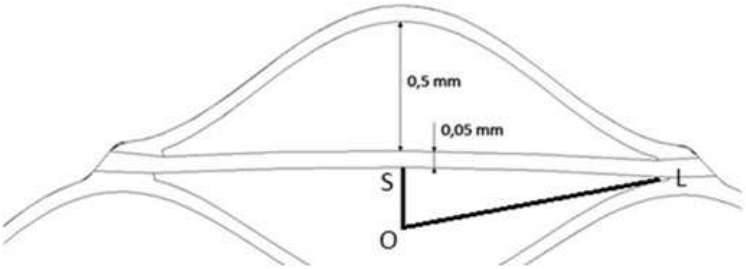

Figure 2: Cross-section of the microchannels in the honeycomb with highlighted characteristic dimensions of thermocatalytic reactor, where short straight $|OS| = 0.184$ mm and long straight $|OL| = 0.834$ mm.

A mathematical model used in solver contains basic governing equations that include continuity, momentum, energy, evolution of kinetic energy of turbulence, evolution of dissipation of kinetic energy of turbulence and species transport. Equations were assumed in a manner showed below.

Firstly, mass balance (continuity) equation is as follows:

$$\frac{\partial}{\partial t}\rho + \mathrm{div}\,(\rho\mathbf{v}) = 0\ , \tag{1}$$

where $\rho{=}\rho(\mathbf{x},t)$ represents the mixture density that depends on gas component m, t and $\mathbf{x}$ are the time and location, respectively, $\mathbf{v}{=}v_i\mathbf{e}_i$ is velocity vector including $\mathbf{e}_i$ – versor in $\boldsymbol{i}$-direction and v_i – value of vector.

Momentum balance equation can be written as

$$\frac{\partial}{\partial t}(\rho\mathbf{v}) + \mathrm{div}(\rho\mathbf{v}\otimes\mathbf{v} + p\mathbf{I}) = \mathrm{div}(\mathbf{t}^t) + \rho\mathbf{S}_\mathbf{v}\ , \tag{2}$$

where $\rho\mathbf{v}$ is the momentum density vector, p represents thermodynamic pressure, $\mathbf{I} = \delta_{ij}\mathbf{e}_i{\otimes}\mathbf{e}_j$ defines unit tensor, δ_{ij} is Kronecker's delta and $\otimes$ denotes the dyadic multiplication. Additionally, total diffusive momentum flux defined as $\mathbf{t}^t = \mathbf{t}^{lam}{+}\mathbf{t}^{tur}$ takes into account two components of viscous stress flux, namely, laminar and turbulent. In Eq. (2) $\rho\mathbf{S}_\mathbf{v}$ is the momentum source.

Energy balance equation reads:

$$\frac{\partial}{\partial t}(\rho e) + \mathrm{div}(\rho e\mathbf{v}{+}p\mathbf{v}) = \mathrm{div}(\mathbf{t}^t\mathbf{v}{+}\mathbf{q}^t) + \rho S_e\ , \tag{3}$$

where e represents total specific energy $e = u{+}\frac{1}{2}\mathbf{v}^2$ with specific internal energy ($u = c_vT$, c_v – specific heat capacity at constant volume, T –

temperature) and specific kinetic energy ($\frac{1}{2}\mathbf{v}^2$). The total diffusive heat flux $\mathbf{q}^t$ includes molecular heat flux and turbulent heat flux. S_e are the energy sources.

Equation for turbulent kinetic energy evolution can be defined as

$$\frac{\partial}{\partial t}(\rho k) + \mathrm{div}(\rho k \mathbf{v}) = \mathrm{div}(\mathbf{J}_k) + \rho S_k \ , \tag{4}$$

where diffusive flux of turbulent kinetic energy k occurs as $\mathbf{J}_k$ and the source of the kinetic energy of turbulence is represented by S_k.

Equation for turbulent dissipation energy evolution can be expressed as

$$\frac{\partial}{\partial t}(\rho \varepsilon) + \mathrm{div}(\rho \varepsilon \mathbf{v}) = \mathrm{div}(\mathbf{J}_\varepsilon) + \rho S_\varepsilon \ , \tag{5}$$

where $\mathbf{J}_\varepsilon$ is the diffusive flux of dissipation of turbulent kinetic energy ε with sources S_ε.

Finally, equation for species transport can be written as follows:

$$\frac{\partial}{\partial t}(\rho Y_m) + \mathrm{div}(\rho Y_m \mathbf{v}) = \mathrm{div}(\mathbf{J}_m) + \rho S_m \ , \tag{6}$$

where Y_m is mass fraction of gas component $m \equiv$ He, CH_3OH, CO, H_2, CH_4, H_2O, CO_2 , S_m is the creation/destruction sources of species m, and $\mathbf{J}_m$ defines the flux of m components of mixture. More detailed description of Eq. (6) is presented in [12,26].

3 Chemical reactions in thermocatalytic reactor based on the intermetallic phase of Ni_3Al

The main products of the methanol decomposition reaction over the Ni_3Al foils are the hydrogen, carbon monoxide and solid carbon deposits. The by-products are carbon dioxide, methane and water [15,27]. In the simplest case, methanol decomposition may be described by the following equation [27,28]:

$$CH_3OH \ \rightarrow CO + 2H_2 \ . \tag{7}$$

If we consider the thermocatalytic microreactor fed by methanol *via* the decomposition reaction, it should be noticed that carbon monoxide and hydrogen, which are the products, can be consumed in the reacting flow *via* the following methanation reaction:

$$CO{+}3H_2 \ \rightarrow CH_4{+}H_2O \ . \tag{8}$$

The carbon monoxide component is converted into carbon dioxide *via* shift reaction. We decided to employ a simplified single-step non-reversible reaction

$$CO{+}H_2O \rightarrow CO_2 + H_2\,. \tag{9}$$

Carbon deposition can be considered through the Boudouard reaction

$$2CO \ \rightarrow C{+}CO_2\ . \tag{10}$$

It should be mentioned that some of the by-products, especially water, can oxidize the Ni_3Al catalyst surface. Based on the papers [25,29], H_2O is the by-product of methanol decomposition and can be used to create the metallic Ni

$$2Ni_3Al{+}3H_2O \rightarrow 6Ni{+}Al_2O_3{+}3H_2 \tag{11}$$

and also can be converted into aluminium hydroxide

$$Al_2O_3{+}3H_2O \rightarrow 2Al(OH)_3\ . \tag{12}$$

It is worth noting that the appearing Ni nanoparticles can be oxidized by H_2O according to the reaction

$$Ni{+}H_2O \rightarrow NiO{+}H_2 \tag{13}$$

and it can then also takes part in the subsequent reaction of a spinel formation:

$$NiO + Al_2O_3 \rightarrow NiAl_2O_4\,. \tag{14}$$

In spite of the that fact, the Al2O3 creation is energetically privileged and is thus preferentially produced on the catalyst surface. According to [11] the oxidization of Ni_3Al preferentially occurs through grain boundaries.

4 Surface source of methanol decomposition and diffusion of components

As has been already mentioned, changes of gas component, $m = 1, 2, .., n$ (n is the number of components), concentration in the mixture due to chemical reactions can be implemented *via* a volumetric or surface source term, S_m, in the species transport Eq. (6). At this point it should be emphasized that numerous problems of the gas-dynamic boundary layer increase as a result of combination with the chemical phenomena that are taking place

in the vicinity of solids. The flow model of chemical reactions, discussed in many papers [12,30] refers to mechanical, thermal and chemical issues of the phenomena occurring in volume. Phenomena occurring on the surface of the combustion chamber are characterized by complete anisotropy. Apart from the volume production of component, S_m, the reaction of the surface absorption also describes chemical kinetics, and therefore they should be treated as some surface source (or discounts) for the gas component [31].

However, the type of by-products suggests that the Boudouard reaction (10) occurs in the performed experimental catalytic test, it is assumed in the numerical simulation that there is no coke creation during microreactor operation and the products of thermocatalytic oxidation are not deposited on the catalyst surface. Hence, to provide a complete CFD model of the surface processes, it will be necessary to consider the additional phenomena similar to presented in [32–36]. It could be helpful in the future works including the growth of carbon nanotubes. In this paper, it is also be assumed that there are no site species involved in the surface reactions (see Eqs. (11)–(14)) and hence only gas phase species are modeled. For modeling purposes only the methanol decomposition reaction is catalytic so it is assumed that the source term, S_{CH_3OH}, for methanol can be formulated in finite volumes strictly adjacent to the microreactor wall. The source of the decomposition of methanol. S_{CH_3OH}, depends on the catalytic properties of the intermetallic phase of the Ni_3Al, and can be expressed via the following equation:

$$S_{CH_3OH} = W_{CH_3OH}\nu_{CH_3OH(\alpha)}q_{(\alpha)} \ , \tag{15}$$

where $\nu_{CH_3OH\ (\alpha)}$ is the molar stoichiometric coefficient for CH_3OH and αth non-reversible reaction and $q_{(\alpha)}$ is the progression level of αth chemical reaction (reaction rate). It should be added that the reaction rate of the methanol decomposition $q_{(\alpha)} = q_{CH_3OH}$ is then usually given as a function of the methanol molar concentration $[X_{CH_3OH}]$ and the forward rate constant $k_{(\alpha)}$. Following [30], a general equation can be written in the form

$$q_{(\alpha)} = k_{(\alpha)} \prod_m [X_m]^{\nu_{m(\alpha)}} \ , \tag{16}$$

where the total stoichiometric coefficient equals $\nu_{m(\alpha)} = \nu''_{m(\alpha)} + \nu'_{m(\alpha)}$; $[X_m]$ is the molar concentration of mth component, $k_{(\alpha)}$ is the constant of progress of the chemical reaction. The stoichiometric matrix coefficients $\nu_{m(\alpha)}$ are integers: $\nu'_{m(\alpha)}$ is the coefficient of the mth component for the progressive αth reaction, of the non-positive value; while $\nu''_{m(\alpha)}$ is the

stoichiometric coefficient for the reverse reaction of the non-negative value.

In processes of methanol decomposition taking place with the presence of 'third body', specifically the Ni_3Al intermetallic phase the rate of reaction $q_{(\alpha)} = q_{CH_3OH}$ determined in formula (16), should be explicitly dependent on the mass participation of the 'third body' by factor α_{cat} [30]:

$$q_{(\alpha)} = \alpha_{cat}[Y_{cat}]k_{(\alpha)} \prod_m [X_m]^{\nu_{m(\alpha)}}, \tag{17}$$

where $[Y_{cat}]$ is the mass concentration of the catalytic material. If, as is often the case, some of the components operate as the 'third body' more effectively than the others, the factors α_{cat} must be taken into account. Contrary, another 'third body' which does not influence the reaction rate should be negligible with the factor $\alpha_{cat} = 0$.

To obtain the volumetric reaction rate, $q_{(\alpha)} = q_{CH_3OH}$, consistent with the volumetric source term, S_{CH_3OH}, the surface reaction rate should be divided by the height of the computational cell adjacent to the microreactor wall (A_{cat}/V_{cell}). Therefore, in the case of thermocatalytic surface reaction the source of decomposition (15) can be finally rewritten in the following way [13]:

$$S_m = W_m \nu_m \Big(k_{cat}[X_m] \frac{A_{cat}}{V_{cell}} \Big), \tag{18}$$

where the forward catalytic rate constant $k_{cat} = \alpha_{cat} k_{(\alpha)}$. Furthermore, for methanol decomposition it is necessary to consider the effect of interaction with Ni_3Al, namely:

$$S_{CH_3OH} = W_{CH_3OH} \nu_{CH_3OH} \Big(k_{Ni_3Al}[X_{CH_3OH}] \frac{A_{Ni_3Al}}{V_{cell}} \Big), \tag{19}$$

where $\nu_{CH_3OH\ (\alpha)}$is the molar stoichiometric coefficient for CH_3OH and αth non-reversible reaction and W_{CH_3OH} molecular mass of methanol. To obtain the volumetric source term, S_{CH_3OH}, the surface reaction rate should be divided by the height of the computational cell adjacent to the microreactor wall (A_{cat}/V_{cell}). It should be added that the source of methanol decomposition S_{CH_3OH} is then usually given as a function of methanol molar concentration $[X_{CH_3OH}]$ and the forward catalytic rate constant k_{cat}.

However, for methanol and others component concentrations, it is necessary to consider the effect of diffusive fluxes, such as ordinary molecular diffusion, in gas channels as well as Knudsen diffusion. As was presented in [13], for the considered geometry of the thermocatalytic microreactor,

Knudsen diffusion is neglected. In general, diffusion flux, $\mathbf{J}_m$, depends on the diffusion velocity, $\mathbf{V}_m$, in the following way:

$$\mathbf{J}_m = \rho Y_m \mathbf{V}_m \ . \tag{20}$$

The best proven closure on $\mathbf{V}_m$ is the Dixon-Lewis' formula [12]

$$\mathbf{V}_m = \frac{1}{\overline{W}} \sum_{m' \neq m}^{NS} W_{m'} \ D_{mm'} \ \frac{\mathrm{grad} X_{m'}}{X_m} - \frac{D_m^T}{\rho Y_m} \frac{\mathrm{grad}\ T}{T} \quad . \tag{21}$$

where $D_{mm'}$ and D_m^T, are coefficients of respectively multicomponents and temperature diffusion, X_m is the mole fraction, $W_{m'}$ is the molecular mass of component $m^{'} \neq m$, $\overline{W}$ is the average molecular mass of components, $\mathrm{grad} X_m$ represents diffusion vector, while T is the temperature in the reactor.

5 Main assumption of calculation

The cross-section of the microchannels in the honeycomb set is presented in Fig. 3, where the discretized space flow with visible refinement of the boundary layer is shown. In the channels with the inlet and outlet coupling the flow under consideration has been divided into some blocks that have been discretized by means of a structured numerical grid, steeply refined in the normal wall direction. Initial tests allowed the use of a numerical grid to ensure that further refinement did not influence the computational results.

The recalculation of the experimental reaction rate and diffusion flux were performed under the following assumptions: 1) constant temperature of the process, 2) monolithic structure of the reactor, 3) conversion parameters as in Tab. 1, 4) geometric dimensions as were presented in Fig. 2. So temperature diffusion part is neglected and only $D_{mm'}$ is considered in numerical way.

However, aspects of the boundary conditions can be also considered by simulation, prepared *via* computational flow mechanics (CFM) calculations [37,38]. Various organic feeds such as methanol, ethanol, and methane may be decomposed as the primary fuel. The methanol and helium mixture composition employed in the present analysis (Tab. 2) have been based on actual experimental data from one of the considered cases.

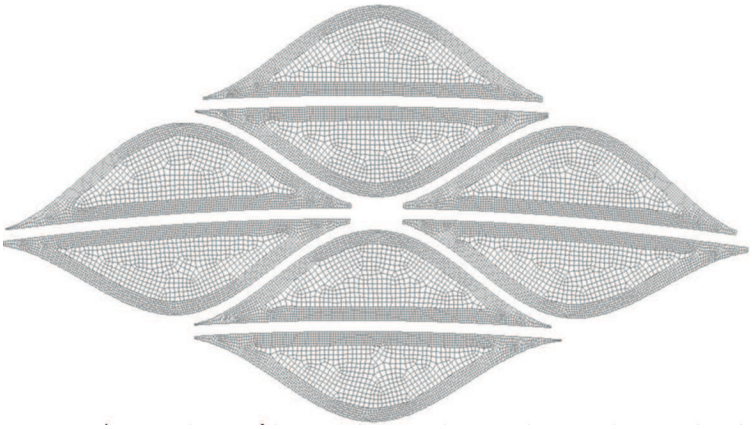

Figure 3: Discretisation by finite volume method of the reacting area.

Table 1: Experimental results of thermocatalytic decomposition over Ni_3Al foil estimated under atmospheric pressure, at velocity 1 cm/s and temperature of the catalysis process 500 °C.

Parameter	Unit	Value
Total mass of catalytic specimens	g	0.777
Density of Ni_3Al foil	g/cm^3	7.51
W/F (weight / flow)	g$_{cat}$s/cm^3	1.48
Conversion of methanol	%	100
Time on stream	h	2
Experimental reaction rate of methanol	g/g$_{cat}$s	1.39

Table 2: Mixture of the methanol and helium composition.

Component	Symbol	Mass fraction [–]
Helium	He	0.158
Carbon	C	0.316
Hydrogen	H	0.105
Oxygen	O	0.421

The velocity was assumed at the level of 1 cm/s (see Tab. 1). It is also known that the lowest possible temperature of the catalysis process which is sufficient to obtain a complete conversion occurred at $T = 500$ °C. For the steady state flow analysis a commercial solver was employed. Finite volume based codes permit one to solve the three-dimensional fluid and heat flow problems concerned with turbulent structures and chemical reactions [39–42]. However, it also allows for the addition of user defined subroutines written in C^{++} for problems that fall outside the capability of the standard version of code. The grid used in the numerical calculations presented here consists of 1 600 000 finite volumes. This enables the model to maintain a high accuracy of results, without consuming unnecessary computing power. In the microreactor, a k-ε turbulent approach was applied due to necessity of utilizing the eddy-dissipation model which was considered as the simplest one to work through using UDF. It has been assumed that the microreactor is adequately isolated, thus assuring an adiabatic condition. It was also assumed that the surface structure of the micro-reactor can be treated as homogeneous.

In this place it should be also added that the structure of microreactor can be treated as an ordered porous structure [43,44], which is quite homogeneous. However, there have been many attempts to analyse heterogeneous porous materials especially when it correlates with a petrophysical parameters [45–48]. Possibilities of modeling this systems using basic law for porous materials can be considered in few approaches: 1) slip flow in porous media [49,50], 2) extension of the Darcy equation for example the Brinkmann-Darcy-Forchheimer equation [51], 3) a model from which one can describe the Klinkenberg effect [52]. For many cases analytical solution is supported by numerical simulation [53], and pore space structure needs new description which is also developed in [54,55].

The standard SIMPLE (semi-implicit method for pressure-linked equations) method has been used for pressure-velocity coupling. The second order upwind schemes have been employed for the solution of the convection term in the governing equations. The diffusion terms have been central-differenced with second order accuracy as well. The detailed methodology of numerical integration regarding the set of governing equations can be found in [12].

6 Results and discussion

Thermocatalytic decomposition of methanol in a single microreactor package is considered as a complicated phenomenon where the main products of the reaction are H_2 and CO (see Eq. (7)). In Fig. 4 is visible that

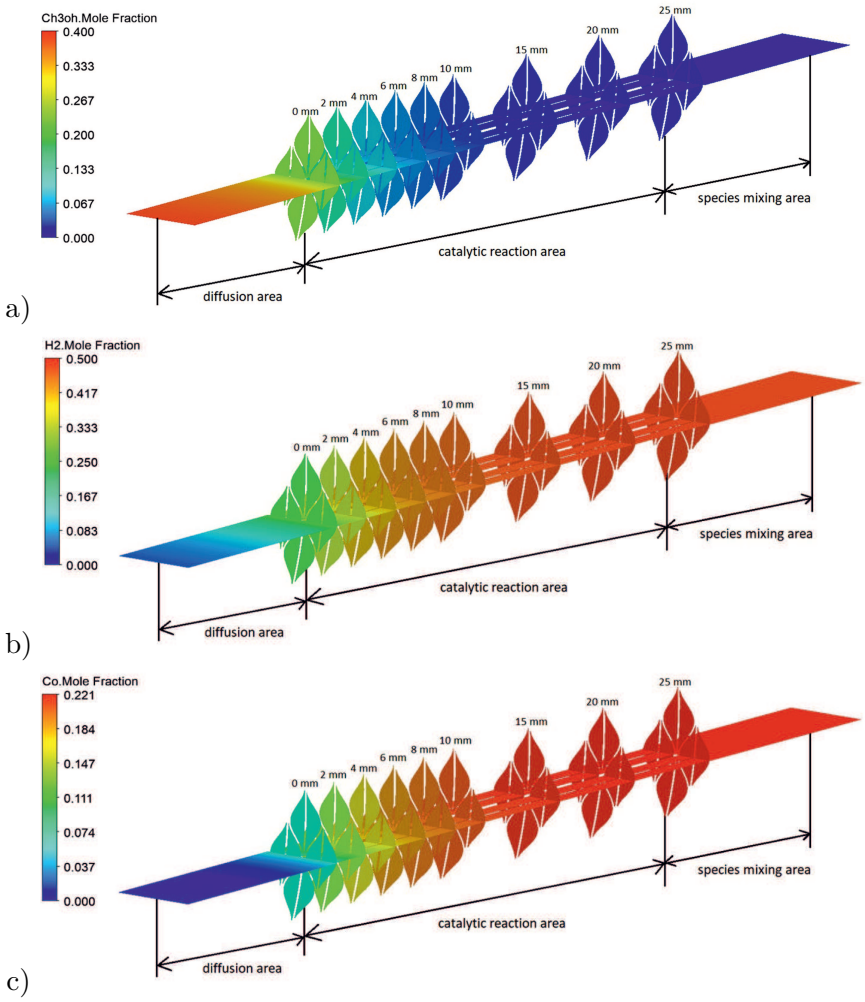

Figure 4: Mole fraction field at eight single microchannels beginning at inlet into the package and terminating at the outlet from the package for: a) methanol, b) hydrogen, and c) carbon monoxide. Thermocatalytic reaction area is located between $L = 0$ mm and $L = 25$ mm.

the two characteristic areas can be distinguished for the whole package:

Firstly, the diffusion flux area before microchannels (between $L = -10$ mm and $L = 0$ mm); secondly, the thermocatalytic reaction area (between $L = 0$ mm and $L = 25$ mm). The maximum of the methanol mole fraction is located at the beginning of the inlet package (see Fig. 4a) and decreases between the centre of the diffusive flux area and the thermocatalytic area in the microchannels, while further diminishing due to the surface catalytic reaction on the Ni_3Al thin foil (conversion of methanol equals 100%).

It should be understood that a decrease of methanol concentration in the diffusion flux area is connected with the diffusion fluxes of the other components, mainly hydrogen and carbon monoxide and mathematically expressed in relations (6) and (20). Mole fraction field at eight single microchannels beginning at inlet into the package and terminating at the outlet from the package for methanol a), hydrogen b), and carbon monoxide c) is presented in Fig.4. A change in the average mole fraction of H_2, CH_3OH, CO, H_2O, CH_4, and CO_2 as a function of the reactor length L is shown in Fig. 5.

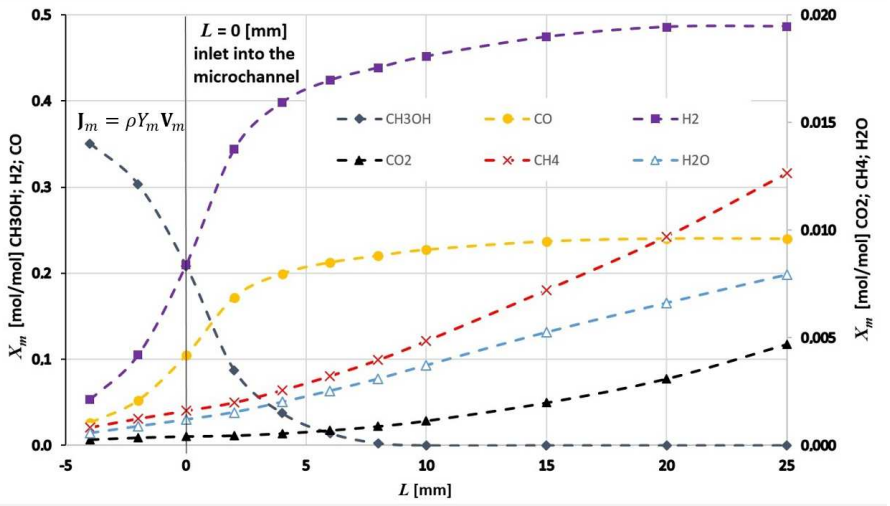

Figure 5: An averaged cross-sectional mole fraction of H_2, CH_3OH, CO, H_2O, CH_4, and CO_2 as a function of the reactor length L. Thermocatalytic reaction area is located between $L = 0$ mm and $L = 25$ mm.

As is highlighted in Figs. 4 and 5, the decrease of CH_3OH and increase H_2, CO concentration from $L = 0$ mm in the direction of the outlet from the package is related directly to the decomposition effects connected with the properties of the intermetallic phase of Ni_3Al. The view of the H_2 mole

fraction change in the axial-sectional which is illustrated in Fig. 5 between $L = -10$ mm and $L = 0$ mm, shows the effects of diffusion.

The estimated average values in the cross section of the CH_3OH mole concentrations have visible tendency towards a changing rate of decrease in mole concentrations as a function of the reactor length L. Similar trends for H_2 and CO increase is correlated with the surface reaction and a strong influence of the diffusion migration of the products of this reaction. Full thermocatalytic decomposition of methanol occurs at $L = 10$ mm into the microchannel from the inlet (Fig. 5), and from this point the volumetric reactions of shifting and methanation reveal a tendency to outweigh the decomposition reactions, however, the mole fractions of H_2O, CH_4 and CO_2 are about ten times lower than the mole fractions of H_2 or CO.

6.1 Influence of the size of honeycomb

Different scales of geometry, namely: small, medium and large have been presented in Fig. 6. The grid used in the numerical calculations presented here consist of 1 600 000 finite volumes for basic geometry case 'small'. For geometry 'medium' and 'large' number of finite elements were accordingly increased, respectively to 2 000 000 and 3 400 000 finite elements (see Tab. 3). This enables the model to maintain a high accuracy of the results, without consuming unnecessary computing power. To compare changes in reaction effectiveness and flow behavior the geometry was scaled firstly by 1.67, and secondly by 2.24. Therefore, once dimensions in every direction were multiplied by 1.67 and after that once again multiplied by 2.24. This way we obtained 3 geometries of the same shape of microchannel but in different sizes. The results of scaling and its effect on reactor volume and mass flow can be seen in Tab. 3.

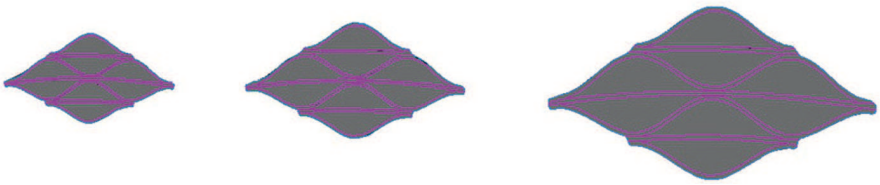

Figure 6: Different scale factor for assumed geometry: small, medium, large, respectively.

The estimated average values in the cross-section of the CH_3OH mole concentrations for different scale factor have been presented in Fig. 7. There

Table 3: Change in parameters (reactor volume and mass flow) for different scale factor for assumed geometry (basic dimensions shown in Fig. 2).

Parameter	Reactor volume [m^3]	Volume multiple [–]	Mass flow rate [kg/s]	Mass multiple [–]
Small	7.04×10^{-08}	1.00	6.29×10^{-08}	1.00
Medium	1.17×10^{-07}	1.67	1.05×10^{-07}	1.67
Large	2.62×10^{-07}	3.73	2.35×10^{-07}	3.73

we have visible tendency towards a changing rate of decrease in mole concentrations as a function of scale factors, mainly large, medium, and small. Full decomposition of methanol is obtained only for the first type of geometry, namely for 'small' size.

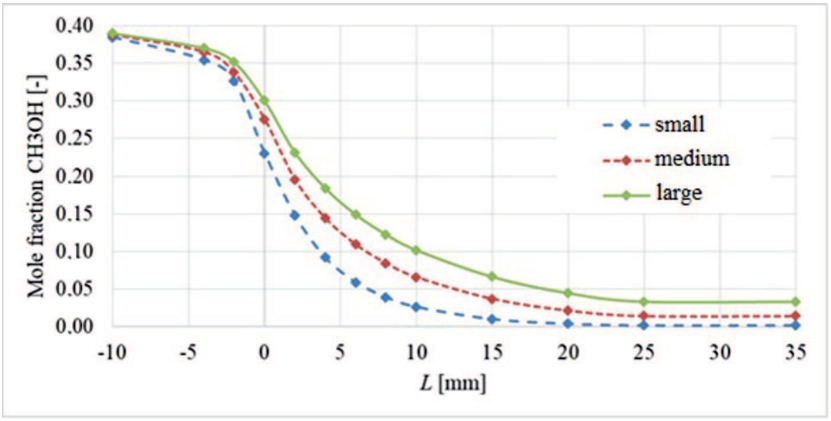

Figure 7: Mole fraction of CH_3OH for different scale factor for assumed geometry. Thermocatalytic reaction area is located between $L = 0$ mm and $L = 25$ mm.

Mole fraction field of CH_3OH for different scale factor for assumed geometry and at the eight single microchannels in the cross sections have been presented in Fig. 8. As can be seen in Figs. 7 and 8 despite significant scale increase the decomposition of methanol still is very effective. Results are as expected, with smaller channels and higher wall influence on the gas flow the decomposition is faster and more complete at the end of the reaction area. Although it is worth to mention that despite significant increase of size (as seen in Tab. 3 almost quadruple in volume) the effectiveness of

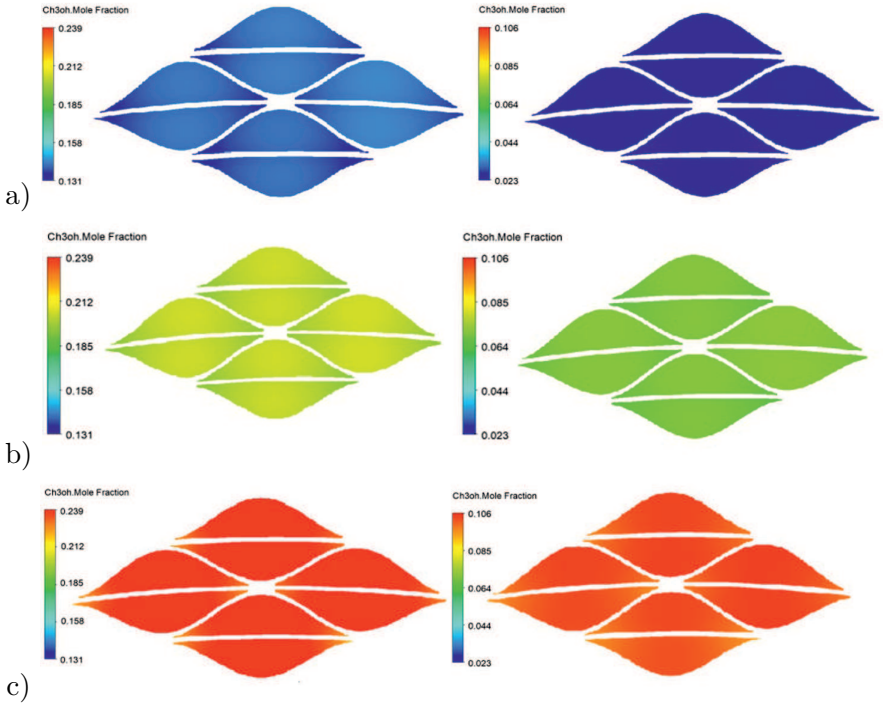

Figure 8: Mole fraction field of CH_3OH for different scale mainly: a) small, b) medium, and c) large; at the eight single microchannels in the cross-sections $L = 2$ mm and 10 mm.

decomposition reaction is still very impressive.

6.2 Velocity field

Velocity field have been presented in Fig. 9. The differences between the selected cross sections, specifically $L = 0$, 2, 10, and 25 mm occur due to thermocatalytic surface decomposition which starts at the inlet to the honeycomb and also because of diffusion effects and volumetric reactions. Hence, with the further increase of the decomposition process, the mixture accelerates due to the increasing number of the mixture moles. The progress of velocity field is rapid through $L = 0$ mm; and consecutive cross-sections $L = 2$, 4, 6, and 8 mm, to the distance about $L = 10$ mm where decomposition is complete. Another process, predominantly mixing due to eddy turbulence, can be observed at the outlet from the microchannels in the honeycomb, $L = 25$ mm.

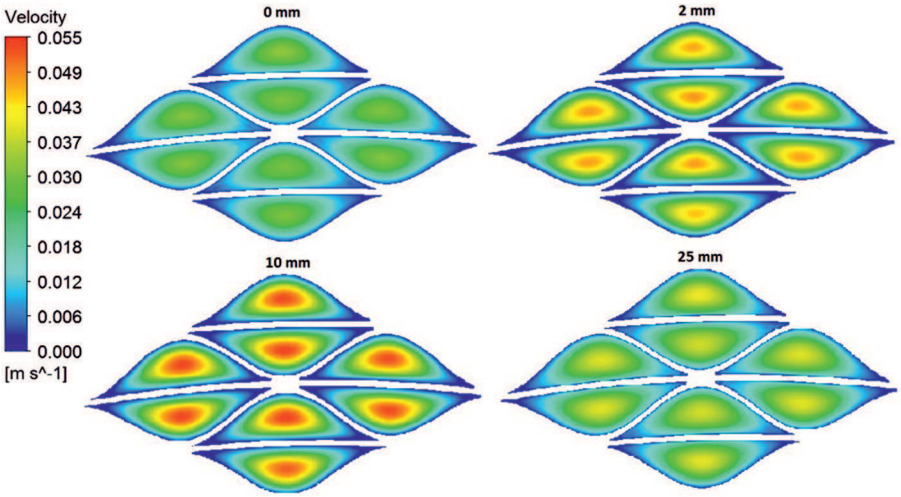

Figure 9: Velocity field at the eight single microchannels in the cross-sections $L = 0$, 2, 10, and 25 mm. Thermocatalytic reaction area is located between $L = 0$ mm and $L = 25$ mm.

7 Conclusions

This paper is concerned with the modeling of hydrogen production by methanol decomposition in the thermocatalytic reactor based on the intermetallic phase of Ni_3Al. Therefore, this article describes the results of interaction between Ni-based foils and the flow which exhibits extremely high catalytic activity in methanol decomposition.

The original methodology of the 3D numerical analysis for thermocatalytic microreactor used in the decomposition of methanol has been presented in this paper. The numerical simulation has been performed *via* cpomputational fluid dynamics (CFD) procedure with extensions including the increased chemical reactions rate at the interphase between fluid and solid. Presented analysis should be considered as one that demonstrated a promising concept in chemical processing possibilities. The data extrapolated *via* the implemented numerical model have made it possible to assess the minimum length of the microreactor channels, which provides an optimal dimension at the system outlet. Results obtained through numerical calculations were calibrated and compared with experimental data to receive satisfactory agreement, however a more sophisticated approach should be considered which includes the effects of deposit growth on the

reaction conditions and temperature field at the wall.

Acknowledgements The work results were obtained in studies co-financed by the National Research and Development Centre in the project PBS 3 ID 246201 titled: 'The development of innovative technology, thin foils of alloys based on intermetallic phase Ni_3Al with high activity thermocatalytic in the field of purification of air from harmful substances or controlled decomposition of hydrocarbons'.

Received 12 December 2018

References

[1] Park S.H., Lee Y.D., Ahn K.Y.: *Performance analysis of an SOFC/HCCI engine hybrid system: System simulation and thermo-economic comparison.* Int. J. Hydrogen Energ. **39**(2014), 1799–1810.

[2] Kalina J.: *Modelling of fluidized bed biomass gasification in the quasi-equilibrium regime for preliminary performance studies of energy conversion plants.* Chem. Process Eng. **32**(2011), 2, 73–89.

[3] Kardaś D., Polesek-Karczewska S., Ciżmiński P., Stelmach S.: *Prediction of coking dynamics for wet coal charge.* Chem. Process Eng. **36**(2015), 3, 291–303.

[4] Çelik D, Yildiz M.: *Investigation of hydrogen production methods in accordance with green chemistry principles.* Int. J. Hydrogen Energ. **42**(2017), 3, 23395–23401.

[5] Chiron F.-X., Patience G., Rifflart S.: *Hydrogen production through chemical looping using $NiO/NiAl_2O_4$ as oxygen carrier.* Chem. Eng. Sci. **66**(2011), 6324–6330.

[6] Martin-Sanchez N., Sanchez-Montero J., Izquierdo C., Salvador F.: *Improving the production of hydrogen from the gasification of carbonaceous solids using supercritical water until 1000 bar.* Fuel **208**(2017), 558–565.

[7] Jóźwik P., Grabowski R. Bojar Z.: *Catalytic activity of Ni_3Al foils in methanol reforming.* Mater. Sci. Forum **636-637**(2010), 895–900.

[8] Jóźwik P, Polkowski W, Bojar Z.: *Applications of Ni_3Al based intermetallic alloys — current stage and potential perceptivities.* Materials **8**(2015), 2537–2568.

[9] Olafsen A., Daniel C., Schuurman Y., Raberg L.B., Olsbye U., Mirodatos C.: *Light alkanes CO_2 reforming to synthesis gas over Ni based catalysts.* Catal. Today **115**(2006), 179–185.

[10] Michalska-Domańska M., Jóźwik P., Jankiewicz B., Bartosewicz B., Siemiaszko D., Stępniowski W.J., Bojar Z.: *Study of cyclic Ni_3Al catalyst pretreatment process for uniform carbon nanotubes formation and improved hydrogen yield in methanol decomposition.* Materials Today: Proc. **3** S(2016), 171–177.

[11] Moussa S.O., El-Shall M.S.: *High-temperature characterization of reactively processed nanostructure nickel aluminide intermetallics.* J. Alloys Compd. **440**(2007), 178–188.

[12] Badur J.: *Numerical Modelling of Sustainable Combustion in Gas Turbines.* Wydawn. IMP PAN, Gdańsk 2003 (in Polish).

[13] Jóźwik P., Badur J., Karcz M.: *Numerical modelling of a microreactor for thermocatalytic decomposition of toxic compounds.* Chem. Process Eng. **32**(2011), 3, 215–227.

[14] Badur J., Ziółkowski P., Kornet S., Kowalczyk T., Banaś K., Bryk M., Ziółkowski P.J., Stajnke M.: *Enhanced energy conversion as a result of fluid-solid interaction in micro- and nanoscale.* J. Theor.. Appl. Mech. **56**(2018), 1, 329–332.

[15] Krawczyk P. Badyda K.: *Two-dimensional CFD modeling of the heat and mass transfer process during sewage sludge drying in a solar dryer.* Arch. Thermodyn. **32**(2011), 4, 3–16.

[16] Badur J., Charun H.: *Selected problems of heat exchange modelling in pipe channels with ball turbulisers.* Arch. Thermodyn. **28**(2007), 1, 65–87

[17] Niedźwiedzka A., Schnerr G., Sobieski W.: *Review of numerical models of cavitating flows with the use of the homogeneous approach.* Arch. Thermodyn. **37**(2016), 2, 71–88.

[18] Furmański P., Seredyński M., Łapka P., Banaszek J.: *Micro-macro model for prediction of local temperature distribution in heterogeneous and two-phase media.* Arch. Thermodyn. **35**(2014), 3, 81–103.

[19] Karwacki J., Nowakowska H., Lackowski M., Butrymowicz D.: *Numerical analysis of evaporation in microchannel under capillary pumping.* Arch. Thermodyn. **36**(2015), 2, 3–25

[20] Ziółkowski P., Badur J.: *On Navier slip and Reynolds transpiration numbers.* Arch. Mech. **70**(2018) 3, 269–300.

[21] Kowalczyk S., Karcz M., Badur J.: *Analysis of thermodynamic and material properties assumptions for three-dimensional SOFC modelling.* Arch. Thermodyn. **27**(2006), 3, 21–38.

[22] Orszulik M., Fic A., Bury T., Składzień J.: *A model of hydrogen passive autocatalytic recombiner and its validation via CFD simulations.* Arch. Thermodyn. **34**(2013), 4, 257–266.

[23] Żymełka P., Nabagło D., Janda T., Madejski P.: *Online monitoring system of air distribution in pulverized coal-fired boiler based on numerical modeling.* Arch. Thermodyn. **38**(2017), 4, 109–125.

[24] Asendrych D., Niegodajew P.: *Numerical study of the CO_2 absorber performance subjected to the varying amine solvent and flue gas loads.* Chem. Eng. Commun. **204**(2017), 5, 580–590.

[25] Xu Y., Ma Y., Sakurai J., Teraoka Y., Yoshigoe A., Demura M., Hirano T.: *Effect of water vapor and hydrogen treatments on the surface structure of Ni_3Al foil.* Appl. Surf. Sci. **315**(2014), 475-480.

[26] Ziółkowski P., Stajnke M., Jóźwik P.: *Modeling of a mixture flow of helium and methanol in thermocatalytic reactor and chemical reactions on the intermetallic phase of Ni_3Al.* Trans. Inst. Fluid-Flow Mach. **138**(2017), 33–73.

[27] Mitani H., Xu Y., Hirano T., Demura M., Tamura R.: *Catalytic properties of Ni-Fe-Mg alloy nanoparticle catalysts for methanol decomposition.* Catalysis Today **281**(2017), 669–676.

[28] Michalska-Domańska M., Bystrzycki J., Jankiewicz B., Bojar Z.: *Effect of the grain diameter of Ni-based catalysts on their catalytic properties in the thermocatalytic decomposition of methanol.* CR Chim. **20(**2017) 156–163.

[29] Xu Y., Yang J., Demura M., Hirano T., Matsushita Y., Teraoka Y., Katsuya Y.: *Catalytic performance of Ni-Al nanoparticles fabricated by arc plasma evaporation for methanol decomposition.* Int. J. Hydrogen Energ. **39**(2014), 13156–13163.

[30] Kuo K.K., Acharya R.: *Applications of turbulent and multiphase combustion.* John Wiley & Sons, New Jersey 2012.

[31] Badur J., Ziółkowski P.J. Ziółkowski P.: *On the angular velocity slip in nano flows.* Microfluid Nanofluid **19**(2015), 191–198.

[32] Ziółkowski P., Badur J.: *A theoretical, numerical and experimental verification of the Reynolds thermal transpiration law.* Int. J. Numer. Method H. **28**(2018),1, 64–80.

[33] Modliński N., Madejski P., Janda T., Szczepanek K., Kordylewski W.: *A validation of computational fluid dynamics temperature distribution prediction in a pulverized coal boiler with acoustic temperature measurement.* Energy **92**(2015), 77–86.

[34] Weber R., Schaffel-Mancini N., Mancini M., Kupka T.: *Fly ash deposition modelling: requirements for accurate predictions of particle impaction on tubes using RANS-based computational fluid dynamics.* Fuel **108**(2013), 586–596.

[35] Badur J., Ziółkowski P., Sławiński D., Kornet S.: *An approach for estimation of water wall degradation within pulverized-coal boilers.* Energy **92** (2015), 142–152.

[36] Ziółkowski P., Stajnke M., Jóźwik P., Bojar Z., Ziółkowski P.J., Badur J.: *Analysis of species diffusion and methanol decomposition source in thermocatalytic reactor based on the intermetallic phase of Ni_3Al for low Reynolds numbers.* J. Physics: Conf. Ser. **1101** (2018), 012050.

[37] Lemański M., Karcz M.: *Performance of lignite-syngas operated tubular solid oxide fuel cell.* Chem. Process Eng. **29**(2008), 233–48.

[38] Ziółkowski P., Hernet J., Badur J.: *Revalorization of the Szewalski binary vapour cycle.* Arch. Thermodyn. **35**(2014), 3, 225–249.

[39] Tesch K., Collins M., Karayiannis T., Atherton M., Edwards P.: *Modelling of two-component turbulent mass and heat transfer in air-fed pressurised suits.* Flow Turbul. Combust. **87**(2011), 55–77.

[40] Ochrymiuk T.: *Numerical analysis of microholes film/effusion cooling effectiveness.* J. Therm. Sci. **26**(2017), 5, 459–464.

[41] Stajnke M., Badur J.: *Catalytic utilization of unconventional fuels in a gas turbine*. J. Phys. Conf. Ser. **1101**(2018), 012038.

[42] Sanz O., Velasco I., Reyero I., Legorburu I., Arzamendi G., Gandia L., Montes M.: *Effect of the thermal conductivity of metallic monoliths on methanol steam reforming*. Catalysis Today **273** (2016), 131–139.

[43] Meng Q.B., Gu Z.Z., Sato O., Fujishima A.: *Fabrication of highly ordered porous structures*. Appl. Phys. Lett. **77**(2000), 26, 4313–4315. https://doi.org/10.1063/1.1332109

[44] Nandiyanto A.B.D., Hagura N., Iskandar F., Okuyama K.: *Design of a highly ordered and uniform porous structure with multisized pores in film and particle forms using a template-driven self-assembly technique*. Acta Materialia **58**(2010), 282–289.

[45] Madejski P., Krakowska P., Habrat M., Puskarczyk E., Jędrychowski M.: *Comprehensive approach for porous materials analysis using a dedicated preprocessing tool for mass and heat transfer modeling*. J. Therm. Sci. **27**(2018), 5, 479-486.

[46] Vafai K., Tien C.L.: *Boundary and inertial effects on flow and heat transfer in porous media*. Int. J.Heat Mass Tran. **24**(1981), 195–203.

[47] Krakowska P., Puskarczyk E., Jędrychowski M., Habrat M., Madejski P., Dohnalik M.: *Innovative characterization of tight sandstones from Paleozoic basins in Poland using X-ray computed tomography supported by nuclear magnetic resonance and mercury porosimetry*. J. Petrol. Sci. Eng. **166**(2018), 389–405.

[48] Puskarczyk E., Krakowska P., Jędrychowski M., Habrat M., Madejski P.: *A novel approach to the quantitative interpretation of petrophysical parameters using nano CT: Example of Paleozoic carbonates*. Acta Geophysica **66**(2018),1453–1461.

[49] Ziółkowski P.: *Porous structures in aspects of transpirating cooling of oxycombustion chamber walls*. In: AIP Conf. Proc. **2077**(2019), 020065. https://doi.org/10.1063/1.5091926

[50] Moghaddam R. N., Jamiolahmady M.: *Slip flow in porous media*. Fuel **173**(2016), 298–310.

[51] Hooman K.: *Heat and fluid flow in a rectangular microchannel filled with a porous medium*. Int. J. Heat Mass Tran. **51**(2008), 5804–5810.

[52] Vignoles G.L., Charrier P., Preux C., Dubroca B.: *Rarefied pure gas transport in non-isothermal porous media: effective transport properties from homogenization of the kinetic equation*. Transport Porous Med. **73**(2008), 211–232.

[53] Sobieski W., Dudda W.: *Sensitivity analysis as a tool for estimating numerical modeling results*. Dry. Technol. **32**(2014), 2, 145–155.

[54] Cieszko M., Kempiński M., Czerwiński T.: *Limit models of pore space structure of porous materials for determination of limit pore size distributions based on mercury intrusion data*. Transport Porous Med. **127**(2019), 433–458.

[55] Cieszko M.: *Macroscopic description of capillary transport of liquid and gas in unsaturated porous materials*. Meccanica **51**(2016), 10, 2331–2352, DOI 10.1007/s11012-016-0368-4.